Proceedings of the 10th International Conference on Asian and Pacific Coasts (APAC 2019) Hanoi, Vietnam, September 25-28, 2019

A process-based sediment transport model for sheet flows with the pickup layer resolved in an empirical way

Tan Weikai[1], Yuan Jing[1]

ABSTRACT:
A two-layer process-based model for predicting the sheet-flow sediment transport under wave-current flows is presented. The whole one-dimensional-vertical (1DV) water column is separated into a pick-up layer and a suspension layer. The pick-up layer is resolved through an empirical way, while the suspension layer adopts Reynolds-averaged Navier-Stokes (RANS) equations coupled with a two-equation $k-\omega$ turbulence closure for flow velocity, and a turbulent diffusion equation for sediment concentration. The instantaneous position of sand bed can be modeled as a linear function of Shields parameter, but as a first test of the model, we apply the measured erosion depth as input. The model also includes the hindered velocity effect due to particle-particle interaction, as well as the turbulence damping effect induced by density stratification. The model is firstly validated against the skewed-flow water-tunnel tests published in O'Donoghue and Wright (2004), which have measurements of velocity, concentration, sand flux and net transport rate. A good model-data agreement indicates that the model may be a promising tool to investigate the sheet-flow sediment transport in coastal environments.

Keywords: sheet flows, two-layer model; sediment transport;

INTRODUCTION

Sediment transport under the sheet-flow condition is still an unresolved question to coastal engineers and researchers. With a high net transport rate, it contributes significantly to the evolution of morphology in coastal areas, the scour of nearshore structures, and etc. Many researches have been conducted over the past few decades, attempting to model the net sheet-flow transport rate correctly. Large-scale morphological formulae are proposed by, e.g. van der A et al. (2013), with some success in predicting the net transport rates, but these models strongly rely on the existing dataset, which is still limited by the insufficiency of full-scale laboratory experiments and on-site measurements. In view of this, more and more process-based models are developed to resolve various mechanisms that give a wave-averaged transport rate, e.g. Fuhrman et al. (2013). Generally, one-phase and two-phase models are extensively adopted to study sheet-flow sediment transport. The former treats the sand as passive substances except for the grain falling velocity. However, the dense sediment suspension inside the sheet-flow layer is against this oversimplified assumption, so most of the existing one-phase models apply a bedload formula to model the transport rate inside the sheet layer. Contrarily, two-phase models are designed to directly resolve the water-sand, sand-sand interactions inside the sheet-flow layer, e.g. Kranenburg et al. (2014). However, the expensive computational cost of two-phase models still limits their applicability in practice, and meanwhile, the closures for various micro-scale stresses need more investigations.

In view of these limitations, the present model separates the water column into two layers, namely a pick-up layer, which is below the initial still sand bed as defined in Dohmen-Janssen (1999) and a sediment-suspension (or simply the upper) layer. With the upper layer resolved as in the classical one-phase approach, the pick-up layer is described by the empirical formulae for both spatiotemporally dependent concentration and velocity. Such treatment for the pick-up layer not only bypasses the complex processes represented in a two-phase model, but also provides greater realism in this region. Similar approaches can be found in Malarkey et al. (2003), which did not incorporate the hindered velocity and turbulence damping effects, and the model setups also slightly differ from the present one. The model is consequently validated against the measurements in oscillatory water tunnel for skewed flows by O'Donoghue and Wright (2004).

MODEL SETUP

[1] Department of Civil and Environmental Engineering, National University of Singapore, 1 Engineering Dr. 2, Block E1A 07-03, Singapore, 117576

N. Trung Viet et al. (eds.), *APAC 2019,*
https://doi.org/10.1007/978-981-15-0291-0_54

The computational coordinates are briefly sketched in Fig. 1, wherein the upper panel gives a schematic plot for the two-layer separation. The bottom of the coordinate z (used for the hydrodynamic part) goes up and down with the bed erosion, and hence is dynamic. On the other hand, the coordinate z_s, applied to simulate the concentration, is physically static. In the panel (a) of Fig. 1, as an example, the dash line represents the initial still sand bed, which becomes $\delta_e(t)$ (the instantaneous erosion depth) under the coordinate z at a given time t, but keeps as 0 under the coordinate z_s. The lower panels show the strategy for the two-layer separation. The velocity profile in the suspension layer is predicted by the one-phase model, whereas inside the pick-up layer, linear interpolation is performed for velocity with the non-slip boundary condition applied at the instantaneous bottom. Differently, the concentration is predicted through the one-phase approach above the reference elevation $z_{s,cr}$, below which, the empirical formula is used for the concentration.

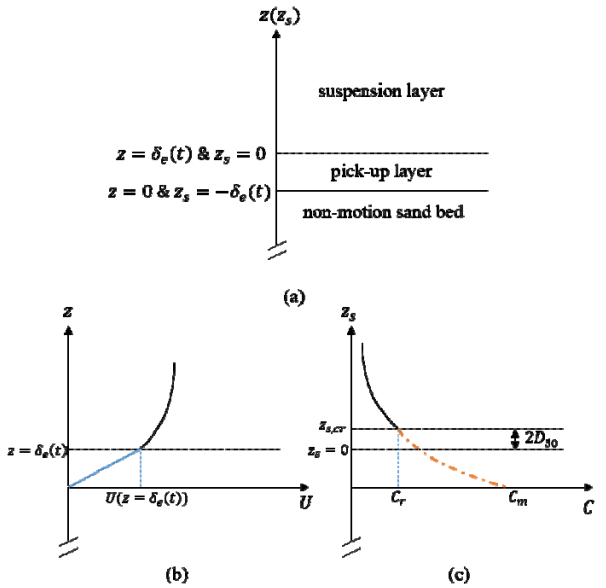

Fig. 1 Schematic sketch of the coordinates used in the simulation. Panel (a) shows the two layers in the model; panel (b) defines the dynamic coordinate z applied to the hydrodynamic part; panel (c) represents the computational domain z_s for predicting the sediment concentration.

The one-phase model for the suspension layer is based on the 1-dimensional-vertical (1DV) Reynolds averaged Navier-Stokes (RANS) equations for the bottom boundary layer. The momentum equation for the horizontal velocity is

$$\frac{\partial u}{\partial t} = -\frac{1}{\rho_w}\frac{\partial p}{\partial x} + \frac{\partial}{\partial z}\left[(\upsilon + \upsilon_T)\frac{\partial u}{\partial z}\right] \tag{1}$$

where u is the horizontal component of velocity, p is the pressure, ρ_w is the density of water, υ and υ_T are molecular and turbulent eddy viscosity, respectively. The turbulent eddy viscosity υ_T is modelled by two-equation $k-\omega$ model, i.e.,

$$\frac{\partial k}{\partial t} = \upsilon_T\left(\frac{\partial u}{\partial z}\right)^2 + \frac{\partial}{\partial z}\left\{\left(\upsilon + \upsilon_T \Big/ \sigma_k \frac{\partial k}{\partial z}\right)\right\} - \beta^* k\omega - B \tag{2}$$

$$\frac{\partial \omega}{\partial t} = \alpha\frac{\omega}{k}\upsilon_T\left(\frac{\partial u}{\partial z}\right)^2 - \beta\omega^2 + \frac{\partial}{\partial z}\left[\left(\upsilon + \sigma\frac{k}{\omega}\right)\frac{\partial \omega}{\partial z}\right] + \frac{\sigma_d}{\omega}\frac{\partial k}{\partial z}\frac{\partial \omega}{\partial z} - c_{3\omega}N^2 \tag{3}$$

with the turbulent eddy viscosity given by

$$\upsilon_T = \frac{k}{\tilde{\omega}} \tag{4}$$

where $\tilde{\omega}$ is,

$$\tilde{\omega} = \max\left\{\omega, C_{\lim}\frac{|\partial u/\partial z|}{\sqrt{\beta^*}}\right\} \tag{5}$$

here $C_{\lim} = 7/8$. In equation (3) σ_d is formulated as,

$$\sigma_d = H\left\{\frac{\partial k}{\partial z}\frac{\partial \omega}{\partial z}\right\}\sigma_{d0} \tag{6}$$

where $H\{\bullet\}$ is the Heaviside step function. The incorporated closure coefficients are given in Wilcox (2008), $\alpha = 13/25$, $\beta = \beta_0 f_\beta$, $\beta^* = 0.09$, $\sigma = 0.5$, $\sigma^* = 0.6$, $\sigma_{do} = 0.125$. On the right hand side of Eq. (2-3), the last terms represent the turbulence damping due to the appearance of stratified fluid-sediment mixture along the water column, where

$$B = \frac{\upsilon_T}{\sigma_p}\left(-\frac{g}{\rho_m}\frac{\partial \rho_m}{\partial z}\right) \tag{7}$$

$$N^2 = B\frac{\sigma_p}{\upsilon_T} = -\frac{g}{\rho_m}\frac{\partial \rho_m}{\partial z} \tag{8}$$

where ρ_m is the density of sand-water mixture, calculated as $\rho_w(1-C)+\rho_s C$, where C is the sediment concentration.

Before giving the boundary conditions to the governing equation, the prescription of wave-current flow in the present model needs to be clarified at first. Conventional way of prescribing wave-current flows is adjusting the pressure gradient term in Eq. (1) iteratively.

However, this is not convenient for flows in Oscillatory Water Tunnel (OWT) due to the lack of a free surface. In this paper, we assume that the modeled water column covers the whole wave boundary layer, but only a very small part of the current boundary layer, see Fig. 2. Therefore, the period-averaged shear stress on the top of the computational domain is approximately equal to the period-averaged (or current) bottom shear stress. Thus in the model, a current is prescribed as a mean bottom shear stress, and the wave is prescribed by an oscillatory pressure gradient.

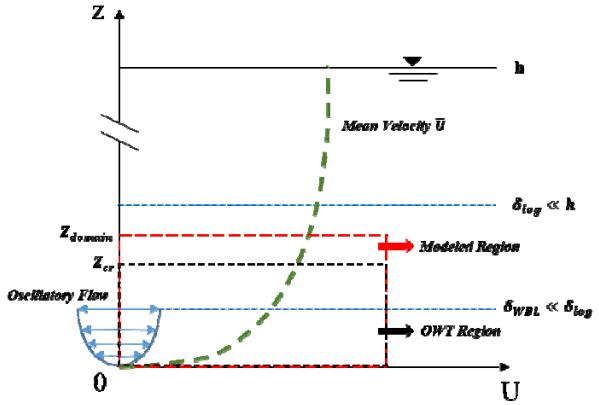

Fig. 2 a conceptual sketch of the computational domain. Z_{cr} is the elevation for reference velocity, $\delta_{\log}$ represents the top edge of the current boundary layer, while δ_{WBL} is the edge of the wave boundary layer. The red box partitions the model's computational domain, while the black box shows a typical testing area in an Oscillatory Water Tunnel.

Since the top of the computational domain is within a logarithmic current boundary layer, the top boundary condition for the horizontal velocity, turbulent kinematic energy k and also the specific rate of dissipation ω are set as,

$$\left.\frac{du}{dz}\right|_{top} = \overline{\tau_{bc}}/(\rho_w \upsilon_T) \tag{9}$$

$$k|_{top} = \frac{u_*^2}{\sqrt{\beta^*}} \tag{10}$$

$$\omega|_{top} = \frac{u_*}{\sqrt{\beta^*}\kappa z_{top}} \tag{11}$$

where u_* is the shear velocity, β^* is an empirical constant in the turbulence model, κ is the von Karman's constant, and z_{top} is at the top boundary. In OWT experiments, current is usually specified as a mean reference velocity $\bar{u}_{cr}$ at a reference level z_{cr}. We initially fit a log profile to the current based on the reference velocity, thus an initial guess of the shear velocity u* is obtained. Then, the value of u* is iteratively changed until the predicted mean velocity matches $\bar{u}_{cr}$ at z_{cr}. The bottom of the model's computational domain is set at the surface of the movable sand bed, where sediment is not in motion. In other words, the datum z=0 is dynamic since the sand bed goes up and down in one wave cycle. Accordingly, the bottom boundary conditions at z=0

$$u|_{z=0} = 0 \tag{12}$$

$$\left.\frac{\partial k}{\partial z}\right|_{z=0} = 0 \tag{13}$$

$$\omega|_{z=0} = \frac{u_*^2 S_R}{\upsilon} \tag{14}$$

where S_R is a function of roughness Reynolds number $k_N^+ = k_N u_* / \upsilon$, with $k_N = 2.5 d_{50}$ (see Wilcox (2006)),

$$S_R = \begin{cases} \left(\dfrac{200}{k_N^+}\right)^2, & k_N^+ \le 5 \\ \dfrac{100}{k_N^+} + \left[\left(\dfrac{200}{k_N^+}\right)^2 - \dfrac{100}{k_N^+}\right] e^{5-k_N^+}, & k_N^+ > 5 \end{cases} \tag{15}$$

As commented by one of the reviewer, the choice of $k_N = 2.5 d_{50}$ may not be physically sound in terms of the sheet flows. We have to admit that taking $k_N = 2.5 d_{50}$ instead of the full roughness allows the calculation to be convenient, and also, many previous studies adopted this method with some success, e.g. Fuhrman et al. (2013). Theoretically, including the turbulence damping effects and movable bottom roughness simultaneously in a model seems to double count some physical processes. Additionally, good model-data agreements for process-based variables, like the velocity and concentration are achieved by adopting $k_N = 2.5 d_{50}$, while some of the existing full roughness formula, e.g. Herrmann and Madsen (2007), does not favor the predictions based on numerical trails. Other than wave-current flows in OWT, this model is also extendable to progressive waves by adding $\partial/\partial x$ terms in left hand side of Eq. (1-3).

The pick-up layer is modelled in an empirical way as shown in Fig. 1. With the non-slip boundary conditions at the bottom, a linear interoperation of the horizontal velocity is performed from the initial still bed to the bottom at each time step t,

$$u(z) = \frac{u(z = \delta_e(t))}{\delta_e(t)} z, \quad 0 < z \le \delta_e(t) \tag{16}$$

while the sediment concentration inside the pickup layer is resolved by an empirical formula proposed by O'Donoghue and Wright (2004),

$$\|C(z)\| = \frac{(z_{cr})^{1.5}}{(z_{cr})^{1.5} + \left(\frac{1}{\|C_r\|} - 1\right) z^{1.5}}, \quad 0 < z \le \delta_e(t) + 2D_{50} \tag{17}$$

where $\|C(z)\|$ is the normalized concentration (against the maximum concentration, usually taken as 0.6) inside the pickup layer, while $\|C_r\|$ is normalized reference concentration, at reference elevation z_{cr}. The reference elevation (under the z coordinate), is set at $\delta_e(t) + 2D_{50}$ above the instantaneous still sand bed ($z=0$). Here the instantaneous erosion depth $\delta_e(t)$ can be modeled as a function of bottom shear stress, e.g., O'Donoghue and Wright (2004). At this stage, the model requires a measurement of $\delta_e(t)$ over a wave cycle as input, but empirical models will be developed in the future to make this model fully predictive. The reference concentration follows the formulation by Chen et al. (2013), who assumed an exponential distribution of suspended sediment from $z=0$ upward. Hence, it gives a reference concentration as,

$$C_r(t) = C_m \exp\left[-\left(1 + \frac{2D_{50}}{\delta_e(t)}\right)\right] \quad \text{at} \quad z_s = 2D_{50} \tag{18}$$

where C_m is the maximum concentration inside the sand bed ($C_m = 0.6$). Above the reference elevation, the sand concentration is depicted by the turbulent diffusion equation,

$$\frac{\partial C}{\partial t} = w_s \frac{\partial C}{\partial z_s} + \frac{\partial}{\partial z_s}\left(D_T \frac{\partial C}{\partial z_s}\right) \tag{19}$$

where w_s is the falling velocity of sand particles, D_T is the diffusion coefficient associated with the turbulence eddy viscosity $D_T = \upsilon_T / \sigma_s + \upsilon$, where σ_s is the Prandtl-Schmidt number, taken as 0.7 according to Breugem (2012). The particle falling velocity is firstly modelled by the formula proposed by Jiménez and Madsen (2003), then modified according to the hindered velocity effect following Richardson and Zaki (1954)

$$w_{s,hindered} = w_s (1 - C)^n \tag{20}$$

where n is determined from,

$$n = \begin{cases} 4.35 R_p^{-0.03}, & 0.2 < R_p < 1 \\ 4.45 R_p^{-0.1}, & 1 < R_p < 500 \\ 2.39, & R_p > 500 \end{cases} \tag{21}$$

here $R_p = w_s D_{50} / \upsilon$ is the particle Reynolds number.

MODEL VALIDATION

A preliminary test of the model's performance is given in this section. Our model does not directly resolve the instantaneous erosion depth at this stage, and hence the measured one is adopted as a model input. O'Donoghue and Wright (2004) focused on skewed oscillatory flows, which has a shorter duration but higher peak velocity during the onshore half-cycle. Hence, the free-stream velocity takes the following form,

$$u(t) = u_1 \sin(\omega t - \varphi_1) - u_2 \cos(2\omega t - 2\varphi_1) \tag{22}$$

where u_1 and u_2 are amplitude of 1st and 2nd harmonics, φ_1 is an adjustment of the phase so that the free-stream velocity always starts from zero during the simulation. In what follows, the validation for the predicted flow velocity, sediment concentration and sand flux will be performed in terms of period-averaged as well as time-varying quantities.

Profiles of velocity, concentration and sand flux at various phases

In order to validate the present model, we perform model-data comparisons for instantaneous profiles. Detailed measurements of velocity and concentration profiles including both accelerating and decelerating phases are available for the dataset of concern at this stage. Hence, as a first test of the model performance, Fig. 2-4, without losing generality, show the profiles for velocity, concentration and sand flux at 4 selected phases for tests FA5010 and MA5010.

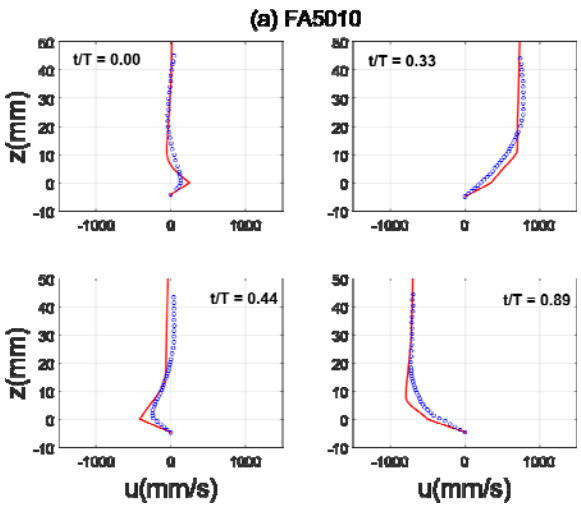

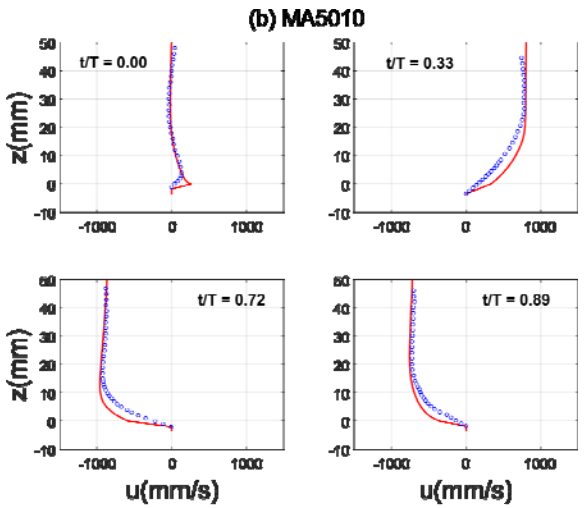

Fig. 2 velocity profiles at the selected phases red solid line represents the prediction, while the blue dots are measurements.

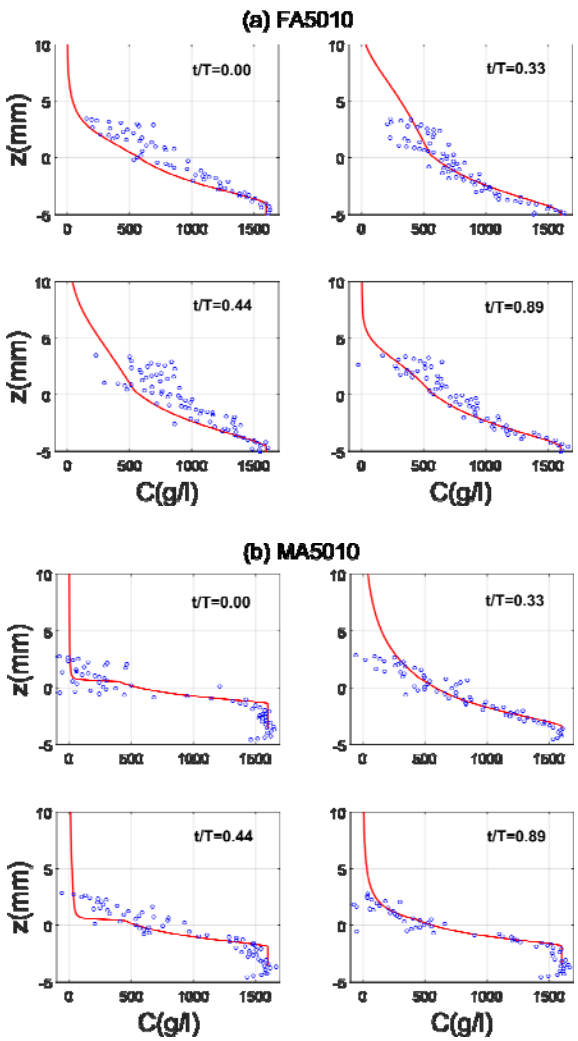

Fig. 3 concentration profiles at the selected phases, solid line represents the prediction, while blue dots are measurements.

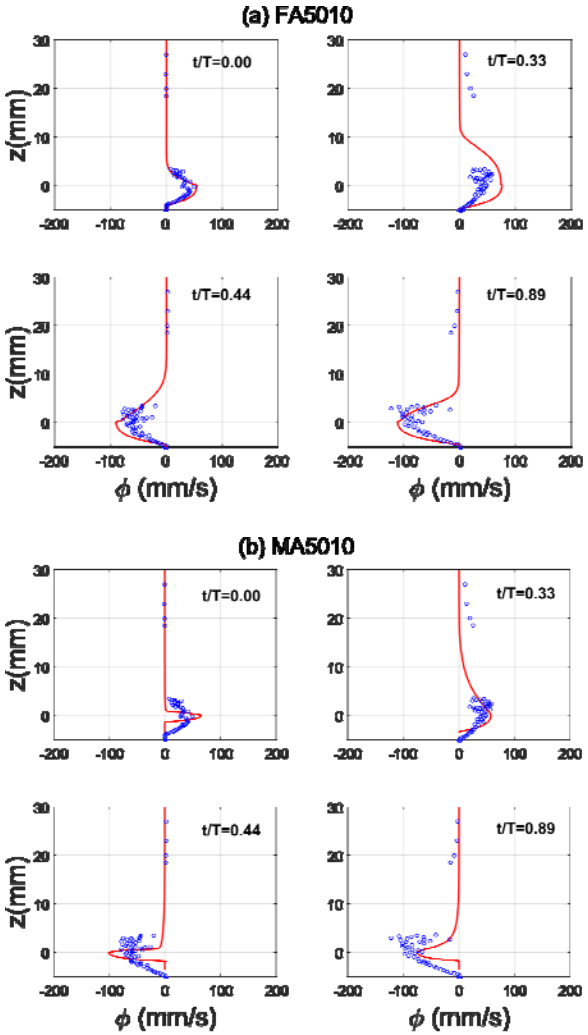

Fig. 4 sand flux profiles at the selected phases, solid line represents the prediction, while blue dots are measurements.

In Fig. 2, the predicted velocity profiles generally follow the measurements for both FA5010 and MA5010. The regions with large velocity gradient are reasonably captured by the present model, illustrating a reasonable reproduction of wave boundary layer, where most of the sediment transport occurs. On top of that, an impressively excellent predictions of the concentration profiles are clearly illustrated in Fig. 3. The accurate estimations of concentration are not only presented in the pick-up layers but also in the upper layers, indicating that both two layers are appropriately resolved. For some profiles, we have to admit that there are kink points due to the two-layer separation, which is an intrinsic limitation of the present model. Smoother results can be obtained by two-phase models, but they are usually more complex than the present one in dealing with the near-bed processes.

The variable that of the most concern is the net transport rate in a coastal sediment transport model. Hence, the instantaneous sand-flux profiles, as a detailed description of the net transport rate at the selected phases, are presented in Fig. 4. The predicted net flux for the fine sand test FA5010 shows a good agreement with the measurements, suggesting the present model decently captures the transport process for the test FA5010. Also shown in Fig. 4 is the test MA5010, although for some of the phases, the model seems to slightly overestimate the magnitude of the sand flux, the overall agreement is still acceptable in terms of modelling the sediment transport. These over predictions may be due to the over-simplified formulizations inside the pick-up layer, wherein inter-phase interactions may reduce the velocity. In effect, over estimations of velocity profiles can be found in the near-bed regions in Fig. 2. Despite of that, the model seems to surpass previous one-phase models, especially for the fine sand case FA5010.

Period-averaged velocity, concentration

Period-averaged quantities play an important role in net sediment transport rate, which is conventionally separated into the current-related and the wave-related components as below,

$$\langle uC \rangle = \langle u \rangle \langle C \rangle + \langle \tilde{u}\tilde{C} \rangle \tag{23}$$

wherein the angle bracket denotes the period averaging and the tilde operator denotes the intra-wave parts. The first term on the right-hand side refers to the current-related sand flux, and the second term is for the wave-related one. It is of interest to look into each term's contribution to the net sand flux, and hence we present the model-data comparisons for both time-averaged velocity and concentration.

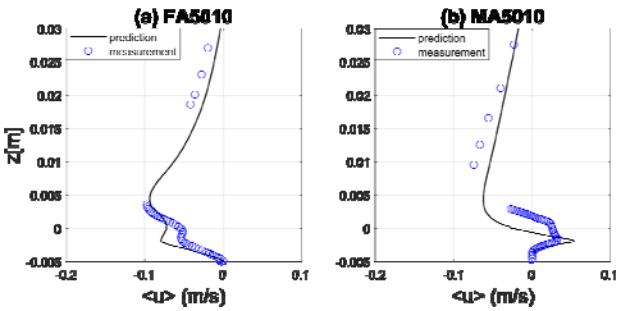

Fig. 5 mean velocity profiles for (a) FA5010; (b) MA5010. Dots are measurements, solid lines are predicted profiles.

In Fig. 5, the predicted mean velocity is compared with the measurements. As discussed in Ribberink et al. (2008), two different modes of the resultant mean velocity profile appear in FA5010 and FA7515 due to the competing of the turbulent-asymmetry boundary layer streaming (TA streaming) and the asymmetry of the intra-wave erosion depth. The former is well recognized for skewed oscillatory flows by many researchers, e.g. the experimental observations by Ribberink and Al-Salem (1995) and analytical solutions achieved by Trowbridge and Madsen (1984). The latter is because the larger erosion depth during the "onshore" half-cycle permits the flow velocity to penetrate into the pick-up layer, while during the "offshore" half-cycle, the penetrated depth is correspondingly less, giving rising to a mean "onshore" velocity in the lower region. As indicated by the Fig. 5, both mechanisms are well captured by the present model. For FA5010, the asymmetry of erosion depth of the two half-cycles is very small due to the small settling velocity, allowing the TA streaming to fully penetrate into the pick-up layer, and contrarily, MA5010 possesses a larger asymmetry for its intra-wave erosion depth, resulting in a positive mean velocity inside the pick-up layer.

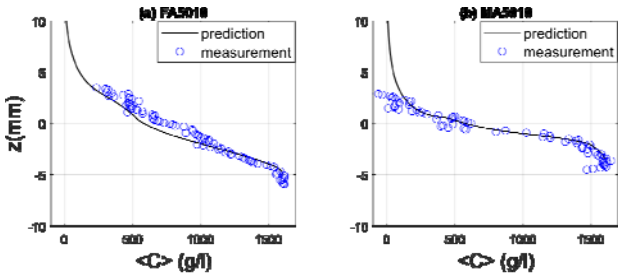

Fig. 6 mean concentration profiles for (1) FA5010; (2) MA5010. Dots are measurements, solid lines are predicted profiles.

Mean concentrations predicted in the bottom region of the computational domain are present in Fig. 6, which reveals an excellent model-data agreement regarding the mean concentration. Again, kink points appear in both cases at the separating points (the reference elevation) due to the two-layer structure of the model. Clearly, both layers produce reasonable predictions. The success of reproducing mean velocity and concentration guarantees that the mean sand fluxes are well predicted by our two-layer model, further suggests the potential of the present model.

Net sand flux and transport rate

The net sand flux is achieved by period-averaged sand fluxes along the water column, it is directly linked to the total net sediment transport rate, which is the depth integral of the net sand flux. For all six skewed-flow tests, the net sand fluxes are shown in Fig. 7. The

left column covers all tests of period 5 seconds, while the right column contains 7.5-seconds tests.

Through comparisons, it is remarkable that the trends of measured net sand fluxes are reasonably captured by the model predictions. For the case FA5010 and FA7515, large negative sand fluxes in the near-bed region are both well predicted, and hence offshore-directed net sediment transport rate can be obtained by our model with a comparable magnitude. The medium-sand and coarse-sand tests have rather noisy measurements of the net sand fluxes at around the initial still sand bed, thus it is difficult to draw conclusions on the accuracy of our predictions. However, it is noteworthy that for the test MA7515, a relative large overshot of net flux inside the pick-up layer is observed, this may cause the over-prediction of the net sediment transport rate. The reason for this deviation is still unknown, and future studies of the present model may tackle upon this issue.

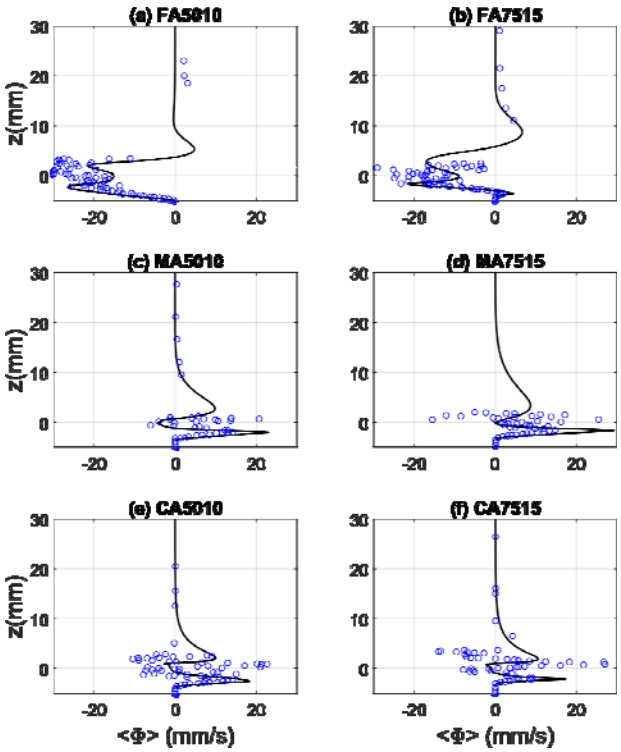

Fig. 7 Net sand flux for six tests. Dots denotes the measurement, solid lines are the predictions.

With a rather good reproduction of the net sand flux over the water column, we also present the depth-integrated value for each case, namely the net sand transport rate. Results are plotted in Fig. 8.

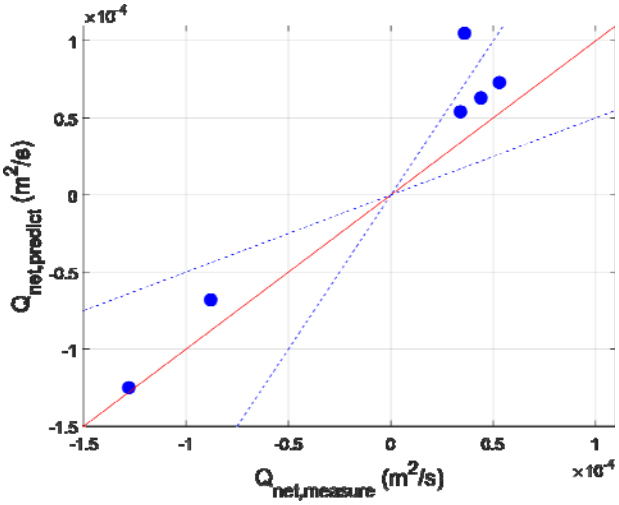

Fig. 8 model-data comparisons of net sediment transport rate. Solid line represents the perfect match, the dash lines represent the bounds of a factor of 2.

As can be expected, the predicted net sediment transport shows a good agreement with the data, excepting for the test MA7515, which is over predicted inside the pick-up layer. We have to admit that there is a tendency that the model overestimates the “onshore” sand transport for medium and coarse sand. One possible reason may be attributed to the oversimplification inside the pick-up layer. On the other hand, the enhanced resistance of the sand bed due to the appearance of a sheet-flow layer, which is not considered in the present settings, may also reduce the net transport rate.

CONCLUSION

A new 1DV sheet-flow model is developed based on a two-layer separation method. With the upper layer modelled by a classical one-phase model, the pick-up layer is resolved in an empirical way. Additionally, turbulence damping and hindered velocity effects are simultaneously incorporated as the basic settings of the model.

The velocity-skewed tests by O'Donoghue and Wright (2004) are applied as a first benchmark of the model. Detailed model-data comparisons are performed for phase-dependent velocity, concentration, and sand flux. Also included in the comparisons are the mean velocity and concentration. These validations give a good understanding of the model behavior, and consequently, the model predicted net sand fluxes are compared to measurements, as a judgement of the model’s accuracy in estimating the net sediment transport rate. As a result, net sand fluxes for two fine-sand cases are well reproduced, while it is difficult to evaluate the medium-sand and coarse-sand tests due to

the noisy measurements at certain levels. The predicted net sediment transport rates are in a good agreement with the measurements, however, a systematic tendency of overestimating the “onshore” transport rates present in the medium-sand and coarse-sand tests. Future studies are required to tackle upon these issues.

REFERENCE

Breugem, W.A., 2012. Transport of suspended particles in turbulent open channel flows, TU Delft, Delft University of Technology.

Chen, X., Niu, X. and Yu, X., 2013. Near-bed sediment condition in oscillatory sheet flows. Journal of Waterway, Port, Coastal, and Ocean Engineering, 139(5): 393-403.

Dohmen-Janssen, C.M., 1999. Grain size influence on sediment transport in oscillatory sheet flow; phase lags and mobile-bed effects.

Fuhrman, D.R., Schløer, S. and Sterner, J., 2013. Rans-based simulation of turbulent wave boundary layer and sheet-flow sediment transport processes. Coastal Engineering, 73: 151-166.

Herrmann, M.J. and Madsen, O.S., 2007. Effect of stratification due to suspended sand on velocity and concentration distribution in unidirectional flows. Journal of Geophysical Research: Oceans, 112(C2).

Jiménez, J.A. and Madsen, O.S., 2003. A simple formula to estimate settling velocity of natural sediments. Journal of Waterway, Port, Coastal, and Ocean Engineering, 129(2): 70-78.

Kranenburg, W.M., Hsu, T.-J. and Ribberink, J.S., 2014. Two-phase modeling of sheet-flow beneath waves and its dependence on grain size and streaming. Advances in Water Resources, 72: 57-70.

Malarkey, J., Davies, A. and Li, Z., 2003. A simple model of unsteady sheet-flow sediment transport. Coastal Engineering, 48(3): 171-188.

O'Donoghue, T. and Wright, S., 2004. Concentrations in oscillatory sheet flow for well sorted and graded sands. Coastal Engineering, 50(3): 117-138.

Ribberink, J.S. and Al-Salem, A.A., 1995. Sheet flow and suspension of sand in oscillatory boundary layers. Coastal Engineering, 25(3): 205-225.

Ribberink, J.S., van der Werf, J.J., O'Donoghue, T. and Hassan, W.N.M., 2008. Sand motion induced by oscillatory flows: Sheet flow and vortex ripples. Journal of Turbulence, 9: N20.

Richardson, J.F. and Zaki, W.N., 1954. Sedimentation and fluidisation: Part i. Chemical Engineering Research and Design, 75: S82-S100.

Trowbridge, J.H. and Madsen, O.S., 1984. Turbulent wave boundary layers: 2. Second-order theory and mass transport. Journal of Geophysical Research: Oceans, 89(C5): 7999-8007.

van der A, D.A. et al., 2013. Practical sand transport formula for non-breaking waves and currents. Coastal Engineering, 76: 26-42.

Wilcox, D.C., 2006. Turbulence modeling in cfd. 3rd edition. DCW Industries, Inc., La Canada, California.

Wilcox, D.C., 2008. Formulation of the k-w turbulence model revisited. AIAA Journal, 46(11): 2823-2838.